Automatic histology registration in application to X-ray modalities

Natalia Chicherova [a,b], Simone E. Hieber [a], Georg Schulz [a], Anna Khimchenko [a], Christos Bikis [a], Philippe C. Cattin [b], Bert Müller[a]

[a] Biomaterials Science Center, Department of Biomedical Engineering, University of Basel, Allschwil, Switzerland;
[b] Medical Image Analysis Center, Department of Biomedical Engineering, University of Basel, Allschwil, Switzerland

ABSTRACT

Registration of microscope images to Computed Tomography (CT) 3D volumes is a challenging task because it requires not only multi-modal similarity measure but also 2D-3D or slice-to-volume correspondence. This type of registration is usually done manually which is very time-consuming and prone to errors. Recently we have developed the first automatic approach to localize histological sections in μCT data of a jaw bone. The median distance between the automatically found slices and the ground truth was below 35 μm. Here we explore the limitations of the method by applying it to three tomography datasets acquired with grating interferometry, laboratory-based μCT and single-distance phase retrieval. Moreover, we compare the performance of three feature detectors in the proposed framework, i.e. Speeded Up Robust Features (SURF), Scale Invariant Feature Transform (SIFT) and Affine SIFT (ASIFT). Our results show that all the feature detectors performed significantly better on the grating interferometry dataset than on other modalities. The median accuracy for the vertical position was 0.06 mm. Across the feature detector types the smallest error was achieved by the SURF-based feature detector (0.29 mm). Furthermore, the SURF-based method was computationally the most efficient. Thus, we recommend to use the SURF feature detector for the proposed framework.

Keywords: Slice-to-volume matching, histology, grating interferometry, phase contrast, synchrotron radiation

1. INTRODUCTION

Image registration as part of medical image analysis plays an important role in clinical research. It helps to improve the accuracy of identifying disease progression and making diagnosis,[1] in both functional and morphological analysis[2,3] and in surgery planning.[4] Extensive research has been done in the field of multi-modal 3D-3D registration for CT, magnetic resonance imaging (MRI) and ultra sound (US).[4–6] Meanwhile, multi-modal registration of two dimensional images to three dimensional data has not been well investigated. However, there is a great need for 2D-3D registration. For example, histological sectioning is the gold standard procedure for tissue analysis in clinics. It is beneficial to determine the position of a histological slide in 3D space such as μCT but only a few papers have addressed this problem.[1,7,8]

The majority of existing methods for 2D-3D registration use various reconstruction techniques.[9–12] They, however, require serial sectioning which is not always available. A single slice to 3D volume alignment, or so called slice-to-volume registration is another type of histology registration.[8,13–17] One of the recent approaches used generalized Hough transform to initialize several slide positions in 3D and then applied affine registration by maximizing mutual information.[7] Wachowiak et al.[18] applied particle swarming optimization to localize 2D slices in reconstructed histology volume. Osechinskiy et al.[19] used intensity based similarity metric for nonrigid slice-to-volume registration. Three classes of spline function were evaluated in histology to MRI registration framework. Slice-to-volume registration proposed by Kim et al.[16] represented coordinates of 2D histological slide in 3D space using non-linear polynomial functions. Due to high complexity of multi-modal registration and

Further author information: (Send correspondence to Chicherova N.)
Chicherova N.: E-mail: natalia.chicherova@unibas.ch

Developments in X-Ray Tomography X, edited by Stuart R. Stock, Bert Müller, Ge Wang, Proc. of SPIE Vol. 9967, 996708 · © 2016 SPIE · CCC code: 0277-786X/16/$18 · doi: 10.1117/12.2237322

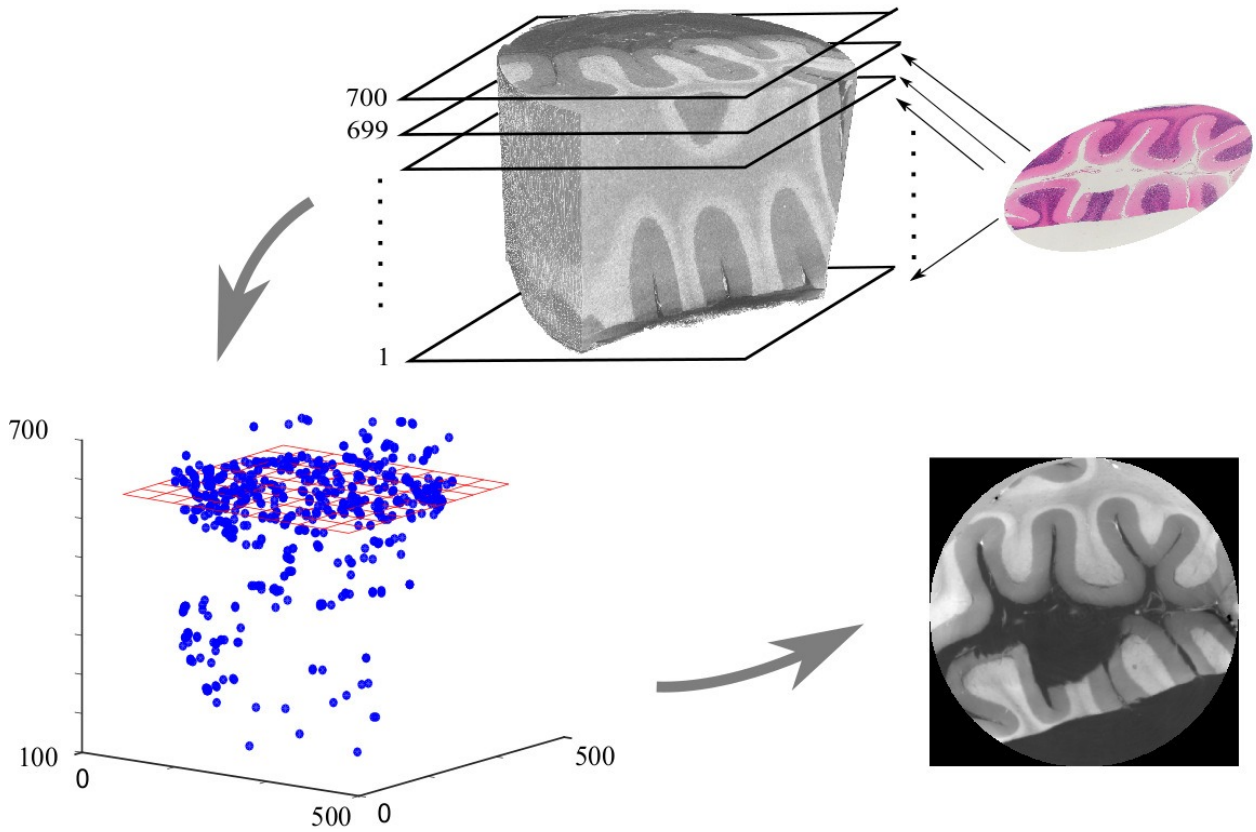

Figure 1. Pipeline of the 2D-3D localization of histology in X-ray dataset. First, histological image is matched with each image in the 3D dataset. The feature point cloud of the 3D dataset is built. Second, the cloud is filtered to remove outliers. Last, the plane is fit to the cloud and a matching image is extracted out of the 3D volume

high number of degrees of freedom, manual intervention is often required at the stage of either segmentation or near ground truth initialization.

In our group we have developed an automatic approach to localize a single histological slide in 3D μCT data (Fig. 1). The main step in the proposed algorithm is robust feature detection and matching. In our previous studies,[20,21] we found that SURF[22] performs best in comparison to SIFT[23] and ASIFT[24] for μCT data of a jawbone. In the current study our goal is to extent the application of the proposed technique to other X-ray based imaging modalities. We analyzed three datasets - grating interferometry (XGI), laboratory-based μCT and single-distance phase retrieval (SDPR) in order to evaluate the method's performance. In addition, we explore other robust feature detectors, so that the best performing parameters can be identified.

2. DATA ACQUISITION

To analyze the performance of the algorithm we use a cylindrical specimen, obtained post-mortem from the cerebellum of a 73-year-old male. The specimen was 6 mm in diameter and 4.5 mm in length. It was extracted from the donated human brain and fixed in 4% histological-grade buffered formalin. The sample was dehydrated and paraffin-embedded according to standard pathology procedures. The cylindrical sample for the tomography measurement was extracted from the paraffin block using a metal punch with an inner diameter of 6 mm.

Grating interferometry (XGI)

High-resolution tomography experiment was carried out in the water tank at the beamline ID19 at the European Synchrotron Radiation Facility (ESRF, Grenoble, France) using a pink beam with a mean X-ray energy 19.45 keV

and effective pixel size 5 μm. Detailed description of instrumentation at beamline can be found elsewhere.[3,25] The interferometer used for the measurement consisted of Si phase grating G_1 with a period of $p_1 = 4.8$ μm and structure height h_1 is 23 μm and Au analyser grating G_2 with a period of $p_2 = 2.4$ μm and structure height h_2 is 50 μm. The intergrating distance was 465 mm, corresponding to the 11^{th} Talbot distance. Grating G_1 was scanned over one period of interference pattern in 3 phase steps, with an exposure time of 2 s per step. The scan was performed over 360° in 1199 angular intervals. The phase recovery and tomographic reconstruction of the data was carried out in Matlab R2014a (MathWorks, Natick, USA).

Laboratory-based μCT

Laboratory-based μCT experiment was carried out using the absorption-contrast μCT system nanotom® m (phoenix|x-ray, GE Sensing & Inspection Technologies GmbH, Wunstorf, Germany) with W transmission target.[26,27] The μCT was performed with a voxel length of 3.5 μm, acceleration voltage 60 kV, e-beam current 350 μA and exposure time 3 seconds. For the acquisition, 1900 projections were recorded over 360°. Measurements were taken in the tube operation mode "0". Data acquisition and reconstruction were performed with datos|x 2.0 software (phoenix|x-ray, GE Sensing & Inspection Technologies GmbH, Wunstorf, Germany). After data reconstruction, the volume was median filtered using VGStudio MAX 2.0 (Volume Graphics, Heidelberg, Germany).

Single-distance phase retrieval (SDPR)

The measurement was performed at the beamline ID19 using pink beam with a mean X-ray energy 36 keV, effective pixel size 3.75 μm, corresponding to a propagation distance of 2.6 m.[28] Over 360° 1500 projection with an exposure of of 0.3 s have been acquired. For the phase recovery we have used the software *ANKAphase*,[28] which implements Pagannin's phase recovery algorithm, with flat field and dark field correction. The ration of decrement of reflective index δ over the absorption coefficient β was set to 2406, corresponding to the value of paraffin. After phase recovery, the tomographic reconstruction of the data was carried out in Matlab R2014a (MathWorks, Natick, USA).
All the 3D datasets were rescaled to the same square image size and resolution of 10.2 μm. The size of XGI datset was $604 \times 604 \times 429$, nanotom μCT was $604 \times 604 \times 101$, and SDPR was $604 \times 604 \times 800$. The length of XGI dataset was 4.4 mm, μCT was 0.4 mm and SDPR was 5.6 mm.

Histological sectioning

After having been scanned in the paraffin cylinder form, the cerebellum sample was re-embedded in a standard paraffin block for subsequent histological sectioning. This was done by partial melting and the addition of fresh paraffin. Starting from the upper part of the sample, tissue sections were obtained using a microtome, left to float on a water bath and then collected one by one and mounted on glass slides. Subsequently, the slides were dried out and stained with haematoxylin and eosin ($H\&E$), following a standard protocol. High-resolution photographs of the slides were taken at 2× optical magnification on a combined light microscope/digital camera system. In total four histological slides were cut. All of the resulting images were converted to greyscale, rescaled, cropped and flipped, as needed.The final resolution of the histological images corresponds to the resolution of 3D datasets, i.e. 604×604 pixels.

3. METHOD

To register a histological slide into a 3D dataset, we proposed a three steps approach (Fig. 1). First, find corresponding feature points between histological slide and each image in the 3D dataset. Second, after storing all the 3D points in a sparse matrix, filter outliers. And last, fit a model of a plane into the filtered 3D point cloud and extract a corresponding image from the 3D dataset.

Feature detection

The image of a histological slide differs from the one of X-ray based modality. One of the main differences is that histological slide is arbitrarily rotated. Therefore, in order to compare it with X-ray image, rotation invariant similarity measure is required. Furthermore, illumination of optical microscopy does not coincide with X-ray acquisition, which requires illumination invariance from similarity measure. Based on these main requirements we have chosen three feature detectors which are invariant to the properties mentioned above, i.e. SURF, SIFT and ASIFT (Fig. 2). The first proposed feature detector SIFT is built on robust extraction of gradient information from an image. Combination of non-maxima suppression in scale pyramid of the image with unstable feature rejection allow for robust feature points identification. The feature points matching is done using descriptor vector. In order to compare the images rotation and illumination invariant descriptor is assigned to each of the feature point. The descriptor determines the main gradient orientations of a neighborhood of the point. Each value of the descriptor vector is represented relative to the dominant orientation of the gradients, which makes it rotation invariant. It is also normalized to account for differences in image's illumination. After constructing the descriptors in two images, the feature points are matched between the images by calculating the distance between the descriptors. If the distance falls into a certain threshold, it is saved as matched. To increase the stability of the matches, we filter the matches in each image that are too close to each other, i.e. the distance is less than 2 pixels. When the matches are very close, they usually have corresponding points that are far from each other in the second image. This means that one of the matches is a certain outlier. By filtering both of them, we might loose one inlier. This however negligible in comparison to the total number of matching points and robustness is favorable. The feature matching algorithm was identical for all three feature detection methods. In the current work we use vlfeat implementation of SIFT algorithm*.

The SURF algorithm is considered as a speed-up version of SIFT. However, the pipeline for feature detection and construction of a descriptor vector noticeably differ from the one of SIFT. The feature detector is based on approximation of Hessian matrix applied to integral images.[29] Moreover, instead of down sampling the image in scale pyramid, the scale space is formed by up-scaling the filter size. The descriptor is built as on Haar-wavelet responses within feature point neighborhood. Moreover, the dimension of the descriptor vector is lower than in SIFT, i.e. 64 and 128 values correspondingly. For the SURF feature detector we use open source code available online †. The number of octaves and initial sampling were set to one. Other parameters were left as default as well as for second nearest neighbour (0.8).

The ASIFT implements affine invariance for feature detection which is not addressed in SIFT. The ASIFT simulates latitude and longitude angles of the camera view so that all six parameters of affine matrix are covered. The additional parameters are then complement SIFT features. The affine deformations between histology image and tomography image is often present especially in soft tissue samples such as cerebellum. The slide thickness is very small so it is almost impossible to retain the same shape after cutting and slide fishing. The code is also available online ‡.

We apply one of the feature detectors to histological image and each image in the X-ray dataset. The matching points of 3D dataset are subsequently stored in a sparse 3D matrix by setting to value to one if the point exist, otherwise zero. After building the 3D sparse representation of the 3D X-ray dataset, we can reduce the registration problem to a density problem. Now the position of the histological slide corresponds to increased density of a feature points in the 3D point cloud.

Plane fitting

The obtained point cloud contains a lot of outliers, therefore, prior to fitting a plane we need to filter the cloud. First, we remove background points by filtering those lying further from the center than $image.size/2.3$. To identify the points that are located in the denser neighborhood we convolve each point with a 3D Gaussian. This allows us to assign higher weights to the points that are more likely to be correct correspondences with the histological image. Then depending on the total number of points, we leave only those with the highest weights.

*http://www.vlfeat.org/overview/sift.html

†http://ch.mathworks.com/matlabcentral/fileexchange/28300-opensurf–including-image-warp-

‡http://www.ipol.im/pub/art/2011/my-asift/

a) SURF

b) SIFT

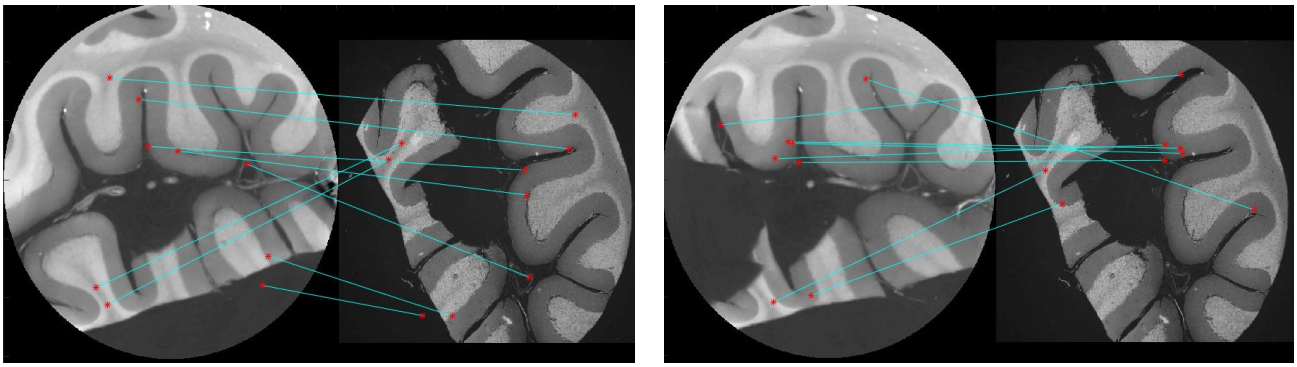

c) ASIFT

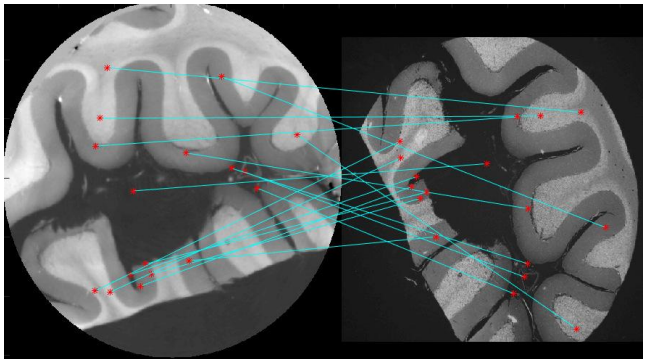

Figure 2. Example of matching points of XGI image and histological image using SURF (a), SIFT (b) and ASIFT (c) as a feature detector.

The filtered point cloud is now used to find a plane that corresponds to the histological sectioning. To fit a model of a plane we use modified version of the RANSAC algorithm.[20,30] RANSAC randomly selects three points out of the 3D point cloud and builds a plane. Than it classifies all the points of the cloud to inliers and ouliers. The inliers are the points that are located within a certain distance from the plane. Similarly, the ouliers are the points further than the distance threshold from the plane. After 15 000 of such iterations, the plane with the highest number of inliers is selected. In order to reduce the search space of possible models of the plane, we constrain the tilting angle. Given approximate range of angles of the histological cut, the correct cutting plane can be allocate with a high accuracy. In our implementation the distance threshold was 10 pixels and the tilting angles were $\alpha_{grat} = \pi/18$, $\alpha_{nanotom} = \pi/28$, $\alpha_{paganin} = \pi/20$.

4. RESULTS

To estimate the accuracy of the proposed techniques, we calculated angle and position differences between automatically and manually found slices. Coordinates of the normal vectors to the planes are first converted to the spherical coordinate system. The obtained vertical distance coordinates of the planes are then subtracted to find the accuracy of the slice localization along vertical axis (Fig. 3 a). The tilting angle was calculated as arccos of a normalized scalar product between the two normal vectors (Fig. 3 b).

Performance of the algorithm on the XGI dataset was significantly better than on the μCT and SDPR datasets (Wilcoxon test p = 0.0012 and p = 0.0011 correspondingly). The average distance error for the XGI dataset did not exceed 0.13 mm. Among different feature detectors, ASIFT showed the smallest median position error (0.06 mm) by accurately localizing all of the histological slides. Moreover, ASIFT was the best at identifying the

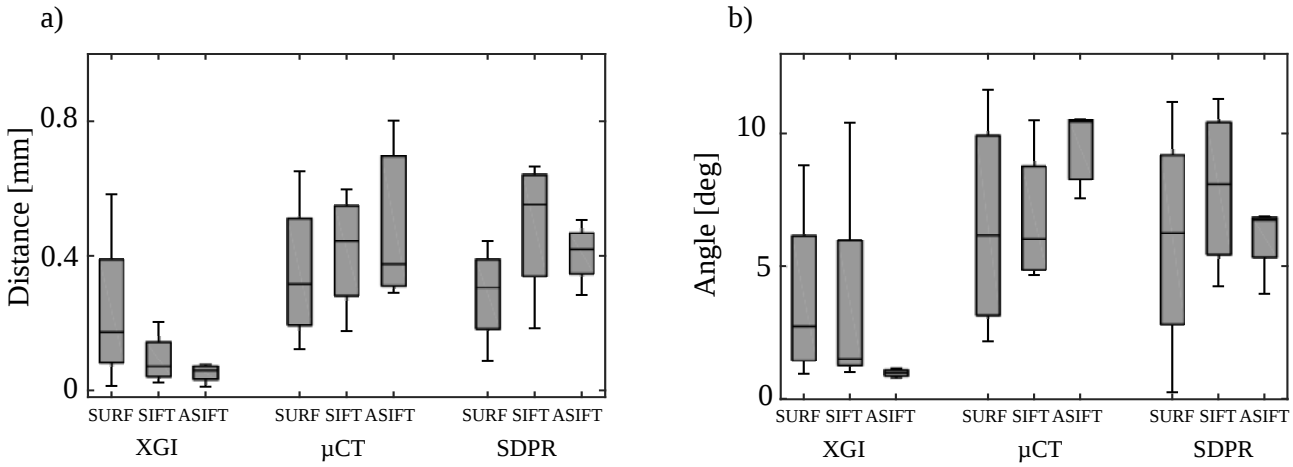

Figure 3. Comparative error for the position (a) and the angle (b) of the plane for three X-ray based imaging techniques. On the x-axis are shown the performance of the SURF- (left), SIFT-(middle) and ASIFT-(right) based methods for each dataset. The median values are shown as black horizontal lines inside the boxes.

angle (median error was less than one degree). ASIFT-based localization did not achieve the same accuracy in μCT (0.6 mm) and SDPR (0.42 mm) datasets and was lower than for SURF-based method (0.3 mm and 0.3 mm correspondingly). Overall, the SURF based feature detection gave better results in the three types of datasets. The total average distance error for SURF-based feature detection was 0.29 mm, for SIFT 0.33 mm and ASIFT 0.41 mm. The difference, however, was not significant (Wilcoxon test $p>0.6$). One slice was excluded from the plot because the ASIFT-based feature detector for the μCT dataset was not able to find a corresponding slice.

In Fig. 4, we show examples of found matching slices for three out of four histological slides. The registration results for the XGI dataset look very similar to the histological slide (Fig. 4 a). All of the feature detectors localized this slide with high precision. In contrast, for the SDPR dataset only SURF- and ASIFT-based registration achieved reasonable results (Fig. 4 b). This slide was particularly challenging because it was cut from the top of the specimen. The 3D datasets did not have enough slices and consequently feature points for robust plane fitting. The laboratory-based μCT dataset had a small size in vertical direction. Therefore, manual and SURF-based slices include black area due to insufficient information for slice interpolation (Fig. 4 c). Nevertheless, the automatically found slices look similar to the ground truth.

5. DISCUSSION

We analyzed the performance of the automatic algorithm that can find position of a single histological slide in a 3D μCT volume proposed in Chicherova et al.[20] Within this framework we evaluated three feature detection algorithms and extended its application to three X-ray based imaging modalities. The highest slide localization accuracy was identified for the ASIFT feature detector applied to grating interferometry dataset. All four histological slides were found with a median error of 0.06 mm. Across the X-ray datasets, the SURF showed the best performance. The average position error was 0.29 mm whereas for the SIFT and the ASIFT it was higher (0.33 mm and 0.41 mm correspondingly).

The main element of the proposed slice-to-volume matching algorithm is a feature detector. The analyzed feature detectors mainly rely on gradient values of an image and perform best for high contrast images. The cerebellum is challenging data for the proposed method because it consists of homogeneous parts of grey and white matter, and consequently low gradient values.[31,32] Therefore, one of the future improvement of the method can be associated with a development of dense multi-modal feature detector. By dense sampling of an image, not only edges will be considered in feature matching, but the entire image. Another challenge is multi-modality of the images. SIFT-based feature detectors are not considered to be suitable for multi-modal matching and initially were made for object recognition. Moreover, due to deformation induced by re-embedding of the specimen, a

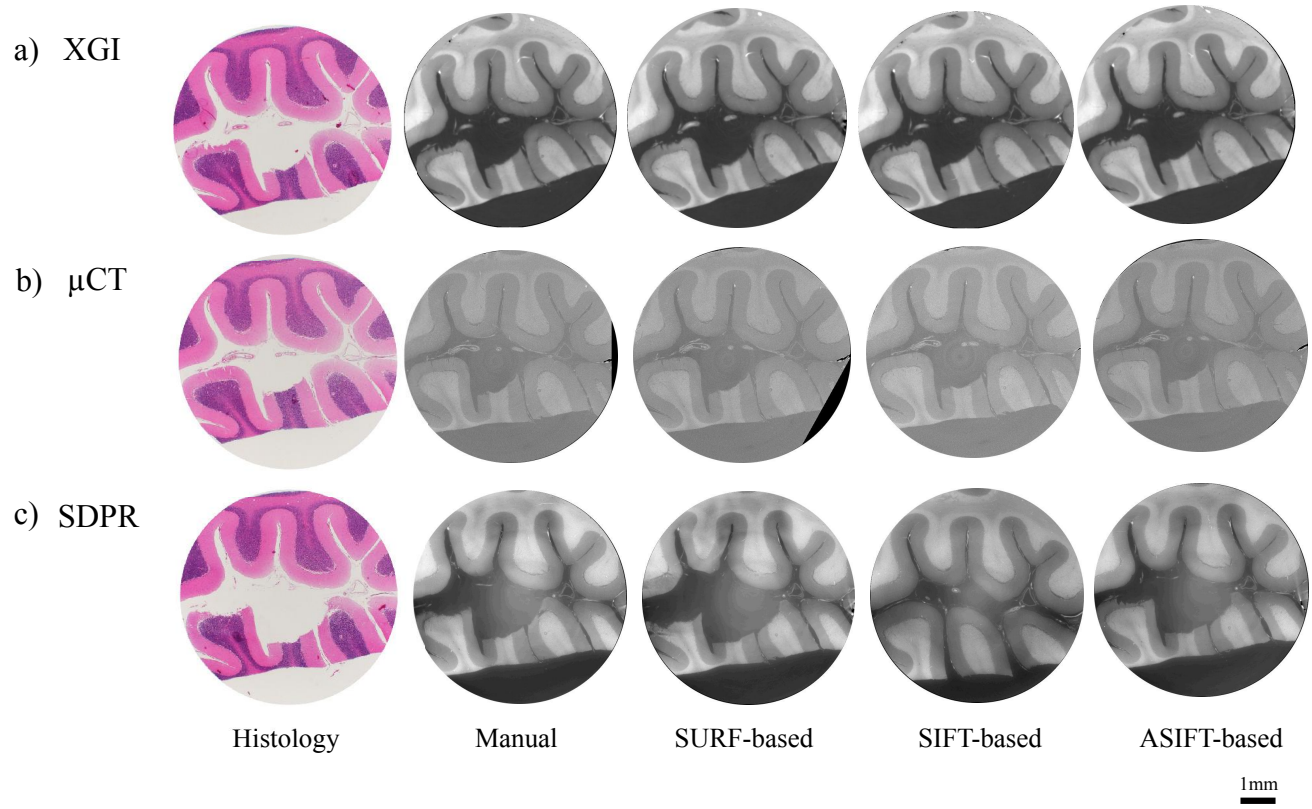

Figure 4. Comparative slice registration for three histological slides (1st column) of three X-ray based acquisition techniques. The resulted tomography slices are found with SURF-(3rd column), SIFT-(4th column) and ASIFT-(5th column) based feature detectors.

plane can not fully match curved surface of a corresponding slice.[31] In spite of all these challenges, the framework gives reasonable results in all of the datasets and shows high potential in application to other imaging modalities such as MRI and US.

The accuracy of slide localization varies from one dataset to another and depends on the feature detectors (Fig. 3). Although the ASIFT applied to the XGI dataset identified histological slides with the highest accuracy it failed to localize a matching slice in the laboratory based μCT. Low contrast of the X-ray images and small vertical resolution did not allow for correct plane fit and the resulting plane lay outside the boundaries of the specimen. Moreover, the 3D feature point cloud obtained with the ASIFT required adaptation of the outlier filtering strategy. The number of feature points for this feature detector was twenty times higher than for the SURF and the SIFT algorithms. Hence, after the second nearest neighbor criteria an additional outlier removal technique could be used (L_1-norm, RANSAC Homography). We conclude that SURF feature detection should be chosen as a general technique in the proposed framework. On average it produces more stable results across different datasets with the lowest error (0.29 mm) and it is faster then other feature detectors. The total time required for localizing a histological image including all feature calculation for the grating interferometry dataset ($604 \times 604 \times 429$) was 75 sec for SURF detector, 101 sec for SIFT and 32 minutes for ASIFT.

To conclude, in this study we explored the parameters of the novel automatic slice-to-volume matching algorithm and extended its application to soft tissue specimen and other X-ray based modalities. The proposed framework showed reasonable performance on a cerebellum sample and across different modalities. All of the analyzed feature detection techniques showed high accuracy in slice localization. Therefore, the proposed method can be used as a general automatic solution for the histology slice-to-volume matching problem.

ACKNOWLEDGMENTS

The work was funded by the Swiss National Science Foundation (SNSF) project 150164 and R'Equip project 133802. Data were obtained with the support of SNSF project CR23I2 125 406 and the ESRF (proposal MD-407).

REFERENCES

[1] Seise, M., Alhonnoro, T., Kolesnik, M., et al., "Interactive registration of 2D histology and 3D CT data for assessment of radiofrequency ablation treatment," *Journal of Pathology Informatics* **2**(2), 9 (2011).

[2] Müller, B., Deyhle, H., Lang, S., Schulz, G., Bormann, T., Fierz, F. C., and Hieber, S. E., "Three-dimensional registration of tomography data for quantification in biomaterials science," *International journal of materials research* **103**(2), 242–249 (2012).

[3] Schulz, G., Waschkies, C., Pfeiffer, F., Zanette, I., Weitkamp, T., David, C., and Müller, B., "Multimodal imaging of human cerebellum-merging X-ray phase microtomography, magnetic resonance microscopy and histology," *Scientific Reports* **2**, 826 (2012).

[4] Markelj, P., Tomaževič, D., Likar, B., and Pernuš, F., "A review of 3D/2D registration methods for image-guided interventions," *Medical Image Analysis* **16**(3), 642–661 (2012).

[5] Zitova, B. and Flusser, J., "Image registration methods: a survey," *Image and vision computing* **21**, 977–1000 (2003).

[6] Pluim, J. P., Maintz, J. A., Viergever, M., et al., "Mutual-information-based registration of medical images: a survey," *Medical Imaging, IEEE Transactions on* **22**(8), 986–1004 (2003).

[7] Hoerth, R. M., Baum, D., Knötel, D., Prohaska, S., Willie, B. M., Duda, G. N., Hege, H.-C., Fratzl, P., and Wagermaier, W., "Registering 2D and 3D imaging data of bone during healing," *Connective Tissue Research* **56**(2), 133–143 (2015).

[8] Sarve, H., Lindblad, J., and Johansson, C. B., "Registration of 2D histological images of bone implants with 3D SRμCT volumes," in [*Advances in Visual Computing*], 1071–1080, Springer (2008).

[9] Ceritoglu, C., Wang, L., Selemon, L. D., Csernansky, J. G., Miller, M. I., and Ratnanather, J. T., "Large deformation diffeomorphic metric mapping registration of reconstructed 3d histological section images and *in vivo* MR images," *Frontiers in human neuroscience* **4**, 43 (2010).

[10] Hallack, A., Papież, B. W., Wilson, J., Wang, L. M., Maughan, T., Gooding, M. J., and Schnabel, J. A., "Correlating tumour histology and *ex vivo* MRI using dense modality-independent patch-based descriptors," in [*Patch-Based Techniques in Medical Imaging*], 137–145, Springer (2015).

[11] Nir, G. and Salcudean, S. E., "Registration of whole-mount histology and tomography of the prostate using particle filtering," in [*Proc. SPIE Medical Imaging*], **8676**, 86760E (2013).

[12] Ourselin, S., Bardinet, E., Dormont, D., Malandain, G., Roche, A., Ayache, N., Tande, D., Parain, K., and Yelnik, J., "Fusion of histological sections and MR images: towards the construction of an atlas of the human basal ganglia," in [*Medical Image Computing and Computer-Assisted Intervention–MICCAI*], 743–751, Springer (2001).

[13] Ferrante, E. and Paragios, N., "Non-rigid 2D-3D medical image registration using markov random fields," in [*Medical Image Computing and Computer-Assisted Intervention–MICCAI 2013*], 163–170, Springer (2013).

[14] Dauguet, J., Delzescaux, T., Condé, F., Mangin, J.-F., Ayache, N., Hantraye, P., and Frouin, V., "Three-dimensional reconstruction of stained histological slices and 3D non-linear registration with *in-vivo* MRI for whole baboon brain," *Journal of Neuroscience Methods* **164**(1), 191–204 (2007).

[15] Goubran, M., de Ribaupierre, S., Hammond, R. R., Currie, C., Burneo, J. G., Parrent, A. G., Peters, T. M., and Khan, A. R., "Registration of *in-vivo* to *ex-vivo* MRI of surgically resected specimens: A pipeline for histology to *in-vivo* registration," *Journal of Neuroscience Methods* **241**, 53–65 (2015).

[16] Kim, T.-S., Singh, M., Sungkara, W., Zarow, C., and Chui, H., "Automatic registration of postmortem brain slices to MRI reference volume," *Nuclear Science, IEEE Transactions on* **47**(4), 1607–1613 (2000).

[17] Schormann, T., Dabringhaus, A., and Zilles, K., "Statistics of deformations in histology and application to improved alignment with MRI," *Medical Imaging, IEEE Transactions on* **14**(1), 25–35 (1995).

[18] Wachowiak, M. P., Smolíková, R., Zheng, Y., Zurada, J. M., and Elmaghraby, A. S., "An approach to multimodal biomedical image registration utilizing particle swarm optimization," *Evolutionary Computation, IEEE Transactions on* **8**(3), 289–301 (2004).

[19] Osechinskiy, S. and Kruggel, F., "Slice-to-volume nonrigid registration of histological sections to MR images of the human brain," *Anatomy Research International* (2010).

[20] Chicherova, N., Fundana, K., Müller, B., and Cattin, P. C., "Histology to μCT data matching using landmarks and a density biased ransac," in [*Medical Image Computing and Computer-Assisted Intervention–MICCAI 2014*], 243–250, Springer (2014).

[21] Stalder, A. K., Ilgenstein, B., Chicherova, N., Deyhle, H., Beckmann, F., Müller, B., and Hieber, S. E., "Combined use of micro computed tomography and histology to evaluate the regenerative capacity of bone grafting materials," *International Journal of Materials Research* **105**(7), 679–691 (2014).

[22] Bay, H., Ess, A., Tuytelaars, T., and Van Gool, L., "Speeded-up robust features (SURF)," *Computer Vision and Image Understanding* **110**, 346–359 (2008).

[23] Lowe, D. G., "Distinctive image features from scale-invariant keypoints," *International journal of computer vision* **60**, 91–110 (2004).

[24] Yu, G. and Morel, J.-M., "Asift: An algorithm for fully affine invariant comparison," *Image Processing On Line* **1** (2011).

[25] Weitkamp, T., Zanette, I., David, C., Baruchel, J., Bech, M., Bernard, P., Deyhle, H., Donath, T., Kenntner, J., Lang, S., Mohr, J., Müller, B., Pfeiffer, F., Reznikova, E., Rutishauser, S., Schulz, G., Tapfer, A., and Valade, J.-P., "Recent developments in X-ray Talbot interferometry at ESRF-ID19," *Proc. SPIE* **7804**, 780406 (2010).

[26] General Electric, Measurement and Control, "phoenix nanotom m 180 kV / 20 W X-ray nanoCT system for high-resolution analysis and 3D metrology," (2014).

[27] Egbert, A. and Brunke, O., "High-resolution X-ray computed tomography for materials research," *Adv. Mat. Res.* **222**, 48–51 (2011).

[28] Weitkamp, T., Haas, D., Wegrzynek, D., and Rack, A., "Ankaphase: Software for single-distance phase retrieval from inline X-ray phase-contrast radiographs," *J. Synchrotron Radiat.* **18**(4), 617–629 (2011).

[29] Viola, P. and Jones, M., "Rapid object detection using a boosted cascade of simple features," in [*Computer Vision and Pattern Recognition, 2001. CVPR 2001. Proceedings of the 2001 IEEE Computer Society Conference on*], **1**, I–511, IEEE (2001).

[30] Fischler, M. A. and Bolles, R. C., "Random sample consensus: a paradigm for model fitting with applications to image analysis and automated cartography," *Communications of the ACM* **24**, 381–395 (1981).

[31] Khimchenko, A., Deyhle, H., Schulz, G., Schweighauser, G., Hench, J., Chicherova, N., Bikis, C., Hieber, S. E., and Müller, B., "Extending two-dimensional histology into the third dimension through conventional micro computed tomography," *NeuroImage* **139**, 26–36 (2016).

[32] Hieber, S. E., Bikis, C., Khimchenko, A., Schweighauser, G., Chicherova, N., Schulz, G., and Müller, B., "Tomographic brain imaging with nucleolar detail and automatic cell counting," *Scientific Reports,* **6**, 32156 (2016).